Topics in Catalysis Vol. 44, Nos. 1–2, June 2007 (© 2007)
DOI: 10.1007/s11244-007-0293-9

Comparison of the activity of Au/CeO_2 and Au/Fe_2O_3 catalysts for the CO oxidation and the water-gas shift reactions

Weiling Deng[a], Colin Carpenter[b], Nan Yi[a], and Maria Flytzani-Stephanopoulos[a,*]

[a]*Department of Chemical and Biological Engineering, Tufts University, Medford, MA 02155, USA*
[b]*Present address: Dartmouth College, Hanover, NH 03755, USA*

We compare the activity and relevant gold species of nanostructured gold–cerium oxide and gold–iron oxide catalysts for the CO oxidation by dioxygen and water. Well dispersed gold nanoparticles in reduced form provide the active sites for the CO oxidation reaction on both oxide supports. On the other hand, oxidized gold species, strongly bound on the support catalyze the water-gas shift reaction. Gold species weakly bound to ceria (doped with lanthana) or iron oxide can be removed by sodium cyanide at pH ≥12. Both parent and leached catalysts were investigated. The activity of the leached gold–iron oxide catalyst in CO oxidation is approximately two orders of magnitude lower than that of the parent material. However, after exposure to H_2 up to 400 °C gold diffuses out and is in reduced form on the surface, a process accompanied by a dramatic enhancement of the CO oxidation activity. Similar results were found with the gold–ceria catalysts. On the other hand, pre-reduction of the calcined leached catalyst samples did not promote their water-gas shift activity. UV–Vis, XANES and XPS were used to probe the oxidation state of the catalysts after various treatments.

KEY WORDS: gold; iron oxide; cerium oxide; CO oxidation; water-gas shift reaction.

1. Introduction

The excitement in the catalysis literature at the discovery of activity of fine particles of gold for a variety of reactions continues unabated ever since it was first reported by Haruta and co-workers [1]. Gold nanoparticles supported on metal oxides can indeed catalyze low-temperature complete oxidation of hydrocarbons and CO, but also epoxidation reactions and hydrogenations, the NO reduction, and several other reactions as has been reviewed in the recent literature [2,3]. Perhaps the most intensively studied reaction to date is the CO oxidation on gold supported on oxides, such as iron oxide and titania [1, 4–7], and ceria [8–11], but also on non-reducible oxides, such as alumina [12–15] and silica [12]. Activity of nanoparticles of gold on non-oxide supports has also been reported [16]. The preferential oxidation of CO (PROX) has been reported to take place on nanoscale gold on oxide supports with high selectivity at temperatures below 120 °C even in realistic fuel gas mixtures [17–19]. In the search for a new generation of low-temperature water-gas shift (WGS) catalysts to replace the low-stability Cu–ZnO, which is unsuitable for fuel cell applications, Au-based catalysts are being actively studied. Again, several support oxides can be used, but reducible oxides are the best. Andreeva's group first showed that Au/Fe_2O_3 is a good WGS catalyst, while our group first reported on the high WGS reaction activity and the merits of Au/CeO_2 catalysts [20].

* To whom correspondence should be addressed.
E-mail: Maria.Flytzani-Stephanopoulos@tufts.edu

Similar to what is known for the Pt-group metals on ceria [21], the presence of gold greatly enhances the reducibility of the surface oxygen of ceria and the WGS reaction lights off at ~100 °C. Nanoscale ceria is much more effective in keeping gold dispersed and in an active state [20,22,23]. A cooperative effect of ceria was invoked to explain why the ceria properties (surface area, crystal size) are crucial both for the Pt-group metals [24] and Au-ceria WGS catalysts [20]. Recently, we were able to document the importance of the interaction between gold and the oxygen of ceria by showing that only the gold species embedded or otherwise associated with ceria [Au_n–O–Ce] are the active sites for the WGS reaction [22,23]. The number of these bound gold species that can be carried by ceria is increased as the crystal size of ceria is decreased [23].

There is conflicting information in the literature about the oxidation state of gold during the dry CO oxidation reaction [4,11,14,15,25–33]. There is also an unresolved issue of the importance of gold particle size for this reaction [5,34,35], while a recent theoretical study finds no effect of the type of oxide support if gold clusters with a large number of cus sites are used [36]. The WGS reaction is much less investigated, but evidence is gradually being collected on the oxidation state of active gold sites, especially on ceria and doped ceria [22,23,37,38], with a theoretical study pointing to stable oxidized gold clusters at ceria oxygen defects as the active sites [39]. The observed reversible reduction/re-oxidation of gold clusters [23,38] as a function of the oxidation potential of the reaction gas mixture is key to our deeper understanding of this system.

In general, the importance of gold–metal oxide interfacial contact has been emphasized in much of the early and more recent reports on CO oxidation reaction [18,40,41]. The coordination of gold to supports is tunable by the reacting mixture composition [31]. Most of the catalysts incorporating Au(0) also contain cationic gold [26,29,42–45] and it is very difficult to separate the function of each. In this paper, we report new data on the catalytic activity and structure of nanoscale Au/Fe_2O_3 and Au/CeO_2 in low-temperature CO oxidation and the WGS reactions. Low-content gold catalysts with oxidized gold species strongly bound to the support were prepared by leaching of parent materials containing both metallic nanoparticles and ionic gold species.

2. Experimental

2.1. Sample preparation

Gold–ceria samples were prepared by deposition precipitation (DP), as described in detail elsewhere [20]. Briefly, lanthana-doped ceria (hereafter as CL) was first prepared by the urea-gelation-coprecipitation (UGC) method [46]. Lanthana was used to stabilize the crystal growth of ceria and maintain high surface area after the calcination step [20,46]. The desired amount of $HAuCl_4$ aqueous solution was added dropwise into a slurry of ceria under constant stirring at room temperature, keeping the pH$\sim$8 by addition of ammonium carbonate. After aging for 1 h, the precipitate was washed with hot (60–70 °C) deionized water three times, dried for 12 h at 100 °C, heated in air at a heating rate of 2 °C/min and held at 400 °C for 10 h. Au/Fe_2O_3 was a commonly used reference material purchased from the World Gold Council (WGC). Leaching of gold from calcined gold–ceria and gold–iron oxide samples took place in an aqueous solution of 2% NaCN under O_2 gas sparging at room temperature and high pH ($\geq$12). After washing by deionized water, the leached catalysts were dried for 12 h at 100 °C and calcined at 400 °C for 2 h. A sample of Fe_2O_3 was prepared by coprecipitation according to a method described by Schubert *et al.* [17] who used it to prepare Au/α–Fe_2O_3. Iron nitrate solution was added dropwise to 500 mL deionized water containing sodium carbonate at pH $\sim$8. The precipitate was washed with water at 60 to 70 °C three times, then dried at 100 °C for 12 h and calcined in air at 400 °C for 2 h.

2.2. CO oxidation and WGS reaction light off tests and kinetic measurements

Steady-state CO oxidation and WGS reaction light off tests and kinetics measurements were conducted at atmospheric pressure with the catalyst in powder form ($<$150 μm). A quartz tube (O.D. = 1 cm) with a porous quartz frit supporting the catalyst was used as a packed-bed flow reactor. Water was injected into the flowing gas stream by a calibrated syringe pump and vaporized in the heated gas feed line before entering the reactor in WGS reaction tests. A condenser filled with ice was installed at the reactor exit to collect water. The feed and product gas streams were analyzed by a HP-6890 gas chromatograph (GC) equipped with a thermal conductivity detector (TCD). For CO oxidation, the gas composition was 2%CO-1%O_2-balance He. The total flow rate was 75 mL/min for light off tests and 150 mL/min for rate measurements. The gas composition for WGS light off tests was 2%CO-10.7%H_2O and 11%CO-26%H_2O-26%H_2-7%CO_2-balance He for the kinetics measurements. In kinetic experiments, the reactor was operated in a differential mode and the typical amount of catalyst used in the tests varied from 10 to 50 mg in CO oxidation and 100 mg in WGS reaction, with the conversion not exceeding 15%.

2.3. Characterization

The BET surface area was measured by single-point N_2 adsorption/desorption cycles in a Micromeritics Pulse ChemiSorb 2705 flow apparatus. Bulk elemental analysis of the samples was conducted by inductively coupled plasma optical emission spectrometry (ICP-OES, Leeman Labs Inc.)

UV–Vis measurements were conducted to identify the oxidation state of gold in iron oxide as prepared and after various treatments. The spectra were recorded by a Hewlett Packard 8452A Diode array spectrophotometer in a wavelength range of 190–820 nm with a resolution of 2 nm. The experiments were conducted in a quartz cell with path length of 1 cm. Gold–iron oxide samples were suspended in ethanol using an ultrasonic bath. This was necessary to achieve an acceptable signal to noise ratio. Background noise was minimized by subtracting the ethanol spectra.

A Kratos AXIS Ultra Imaging X-ray Photoelectron Spectrometer (XPS) with a resolution of 0.1 eV was used to determine the atomic metal ratios of the surface region and the oxidation state of gold in selected catalysts. Samples in powder form were pressed on a double-sided adhesive copper tape for analysis. An Al K_α X-ray source was used in this work. All binding energies were adjusted by using C1s as internal standard.

Synchrotron-based X-ray absorption spectroscopy (XAS) was employed to examine the oxidation state of 0.5AuCL and 0.7$AuFe_2O_3$ under different treatments. XAS spectra were collected using the beamline X19A of the National Synchrotron Light Source (NSLS) at Brookhaven National Laboratory (BNL). Each catalyst sample was pressed on a Kapton tape as a thin film and the XAS spectra were taken in the "fluorescence-yield model". A Ge 13-element detector was used. The reported data are the averages of three scans (lasting approximately 30 min/scan), and no changes were detected between the first and the last scan.

3. Results and discussion

CO oxidation activity data for gold–metal oxide catalysts reported in the literature vary by several orders of magnitude. This has been attributed to differences in the preparation method as well as to different reaction conditions employed. Table 1 summarizes the performance of some of the most active catalysts reported in the literature for the CO oxidation over Au-metal oxide catalysts, including data from this work.

The physical properties of the gold catalysts tested in this work are shown in table 2. The samples reported here are denoted as x Au, where x is the atomic percent of gold, using the total amount of metals as the basis.

3.1. CO oxidation on Au/CeO_2

Among the reducible oxide supports of gold catalysts, ceria is very important. It has been reported that formation of reactive oxygen species on nanocrystalline ceria is enhanced by the presence of gold [27,50]. Gold on nanoscale ceria is two orders of magnitude more active for the CO oxidation reaction than if deposited on microcrystalline ceria [11]. In this work, ceria was doped with 10 at.% lanthanum, which inhibits the crystal growth of ceria during the calcination step [20,46]. Gold deposited on CL is very active for CO oxidation [9,10]. Figure 1 shows light-off curves for 4.7AuCL and leached 0.5AuCL catalysts in a CO oxidation reaction gas mixture containing 2%CO-1%O_2 in He. The space velocity is 100,000/h. The 4.7AuCL sample containing metallic gold nanoparticles has high activity for CO oxidation, even at temperatures below RT, while 0.5AuCL, which contains only oxidized gold clusters, lights off above room temperature. The two catalysts fully oxidize the CO at ~110 °C. To check whether the activity of the 0.5AuCL sample is a result of part of its gold being reduced during the ascending temperature tests, the CO conversion over 0.5AuCL at 75 °C and 50 °C was retested in situ in descending temperature mode. As shown in figure 1 there was no hysteresis, indicating that the sample had not changed during the testing. Thus, the oxidized gold species, $Au_n^{\delta+}$, have distinct activity for the CO oxidation reaction, much lower than that of Au^o. The rates of the reaction and apparent activation energies are shown in table 1. The nanoscale ceria (CL sample) was also tested for comparison. As shown in figure 1, this is much less active than the gold-containing ceria catalysts. In a recent FTIR study of CO adsorbed on a similar set of parent and leached gold–ceria samples, it was found that CO

Table 1
CO oxidation activity of Au-metal oxide catalysts

Catalyst	Preparation	Au (wt%)	CO: O_2	Reaction rate at 30 °C (mol CO/g_{cat}/s)	Ea (kJ/mol)	Reference
Au/α–Fe_2O_3	CP	3.15	1:1	5.1E-6	31	17
Au/α–Fe_2O_3	CP	0.66	1:20	1.1E-6	35.3	18
Au/α–Fe_2O_3 [a]	CP	2.0[b]	2:1	8.9E-6	13.4	This work
Au/α–Fe_2O_3	CP, leached	0.7[b]	2:1	3.5E-6 at 200 °C	32.6	This work
Au/α–Fe_2O_3	CP, leached, then reduced in H_2 at 400 °C	0.7[b]	2:1	1.3E-5 at 20 °C	9.9	This work
$Au/Fe(OH)_3$	IMP	3	1:20	1.5E-5	15	47
Au/CeO_2	DP	3	1:1	6E-6 at −10 °C	N/A	48
Au/CeO_2	DP	1.5	1:20	1.7E-6	N/A	35
Au/CeO_2	Combustion	0.85	1:1	2.3E-7	N/A	36
Au/CeO_2	DP	2.8	0.2 CO: 19.8 air	3E-6 at 5 °C	12[c]	11
AuCe(La)Ox	CP	5[b]	1:1	1.2E-6 at 31 °C	53.7	9,10
AuCe(La)Ox	DP	4.6[b]	2:1	1.8E-6 at 25 °C	41.1	49
AuCe(La)Ox	DP, leached	0.2[b]	2:1	1.8E-5 at 100 °C	39.5	49
AuCe(La)Ox	DP	4.7[b]	2:1	1.3E-5	29.5	This work
AuCe(La)Ox	DP, leached	0.5[b]	2:1	3.7E-6 at 50 °C	50.8	This work
AuCe(La)Ox	DP, leached, then reduced in H_2 at 400°C	0.5[b]	2:1	8.1E-6 at 50 °C	39.9	This work
Au/TiO_2	CP	3.3	1:20	1.7E-5	34.4	18
Au/TiO_2	DP	3.1	1:20	2.0E-5	27	4
Au/TiO_2	CP	2.4	1:1	3.0E-6	31.1	40
Au/Al_2O_3	DP	1.16	0.3–7%CO and O_2	8.9E-7	12	14
Au/Al_2O_3	DP, NaCN	0.16	0.3–7%CO and O_2	1.5E-7	18	14
Au/Al_2O_3	IMP	0.30	3.3:1.7	7E-6 at 300 K	N/A	15
Au/SiO_2	CVD	6.6	1%CO in air	1.5E-6 at 273 K	17	12
Au/SiO_2	IMP	1	3.3: 1.7	8.1E-7 at 300 K	N/A	15

[a]material purchased from the World Gold Council.
[b]in atomic percent.
[c]calculated from the rate data.

Table 2
Physical properties of gold–ceria and gold–iron oxide materials

Sample	Preparation	BET Surface area (m^2/g)	Surface composition[a] (at.%)			Particle size[b] (nm)		Bulk composition[c] (at. %)		
			Au	Ce or Fe	La	Au	CeO_2 or Fe_2O_3	Au	Ce or Fe	La
4.7AuCL	DP	146.3	4.66	79.16	16.18	5.0	5.1	4.7	85.8	9.5
0.5AuCL	DP, NaCN	161.6	0.70	83.21	16.09	ND	5.1	0.5	89.5	10.0
CL	UGC	156.9	0	NM	NM	NA	4.7	0	92.6	7.4
$2AuFe_2O_3$ [d]	CP	44.2	3.14	96.86	0	5.0	25.6	2.0	98.0	0
$0.7AuFe_2O_3$	CP, NaCN	41.1	ND	100	0	ND	28.5	0.7	99.3	0
Fe_2O_3	CP	58.9	0	100	0	NA	9.0	0	100	0

All samples calcined at 400 °C in air for 10 h, except leached samples for 2 h; ND: non-detectable; NA: not available; NM: not measured.
[a]Surface composition was determined by XPS.
[b]The crystallite size was calculated by XRD with the Scherrer equation.
[c]Bulk composition was determined by Inductively Coupled Plasma (ICP) spectrometry.
[d]obtained from the World Gold Council.

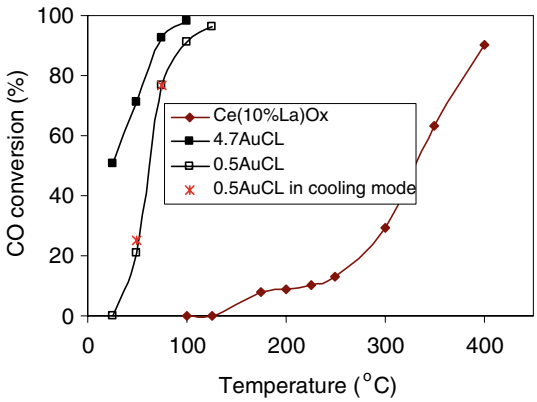

Figure 1 CO conversion in the CO oxidation over gold–ceria catalysts. Gas mixture: 2%CO-1%O_2-balance He; space velocity: 100,000/h.

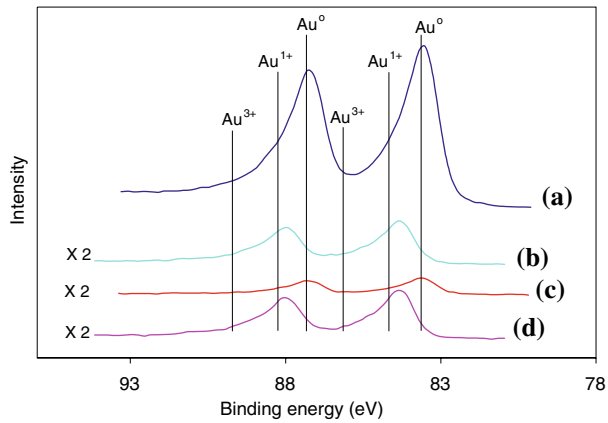

Figure 2 XP spectra of Au_{4f} in as-prepared and used gold–ceria catalysts. X2 represents signal magnification, (a) 4.7AuCL; (b) 0.5AuCL after CO oxidation up to 125 °C (see figure 1); (c) 0.5AuCL, reduced in hydrogen up to 400 °C; (d) fresh 0.5AuCL.

adsorbs more strongly on $Au_n^{\delta+}$ clusters and its reactivity with $^{18}O_2$ gas is lower than that of CO bound (less strongly) on Au^o [51].

The oxidation states of gold in fresh and used catalysts were probed by XPS (Au_{4f}) as shown in figure 2. Lines d and b are for the leached 0.5AuCL material, fresh (line d) and used (line b) after CO oxidation up to 125 °C. Both fresh and used samples have very similar spectra, indicating that the surface structure of gold–ceria is retained during CO oxidation up to 125 °C, in agreement with figure 1. In both samples, gold is present in oxidized state. i.e., oxidized gold species have low activity for the CO oxidation reaction. The fresh leached material shows a 0.2 eV red shifted binding energy of Au^{1+} (84.6 eV [19]). This shift can be explained by initial-state effects. It has been estimated that a negative initial state contribution can be up to 0.6 eV for very small clusters [52]. Corroborating the XPS data, in figure 3 the Au L_{III}-edge X-ray absorption near edge structure (XANES) spectra of both the fresh 0.5AuCL and the one used after CO oxidation up to 125 °C shows the presence of cationic gold [30].

The 0.5AuCL catalyst was treated in 20%H_2- He gas up to 400 °C. Upon this reduction, the gold binding energies shifted to lower values, implying some oxidized gold was reduced to zerovalent gold (Line c in figure 2). Figure 3 also provides evidence of the transformation of cationic gold to Au^o after this reduction. The CO oxidation reaction rates over this reduced 0.5AuCL are twice as high as the fresh catalyst, as can be seen in table 3. Thus, again we find that the presence of Au^o is required to boost the activity. The 4.7AuCL sample containing a large fraction of gold nanoparticles is about seven times more active than 0.5AuCL for the CO oxidation reaction at 50 °C. The apparent activation energies of the reaction, listed in table 4, are different for 4.7AuCL (29.5 kJ/mol) and 0.5AuCL (50.8 kJ /mol) potentially indicating the difference in the activation mechanism of oxygen on the two samples. The reduced 0.5AuCL has intermediate activity between the leached and parent samples, which is reasonable since it contains fewer active sites than the parent catalyst.

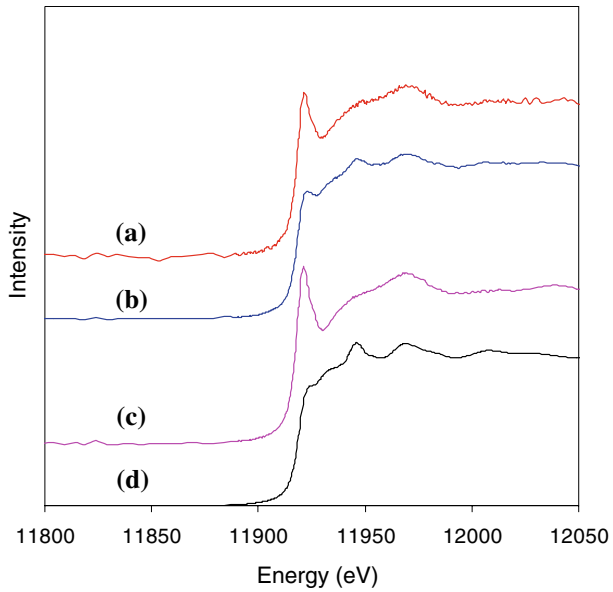

Figure 3 XANES of 0.5AuCL. (a) 0.5AuCL, after CO oxidation to 125 °C (see figure 1); (b) 0.5AuCL, reduced in hydrogen at 200 °C; (c) fresh 0.5AuCL; (d) reference material Au foil.

Table 3
CO oxidation reaction rates over 0.5AuCL[a]

Pretreatment	Temperature (°C)	CO oxidation reaction rate (μmolCO/g_{cat}/s)
Fresh	50	3.74
	40	2.02
Reduced	50	8.12
	40	3.96

[a]See table 2 for sample properties Gas composition: 2%CO-1%O_2-He.

Table 4
Apparent activation energies of the CO oxidation reaction over gold–ceria and gold–iron oxide

Catalyst[a]	Apparent activation energy Ea (kJ/mol)
4.7AuCL	29.5
0.5AuCL	50.8
Reduced 0.5AuCL	39.9 ± 1.4
CL	70.2
$2.0AuFe_2O_3$	13.4 ± 0.4
$0.7AuFe_2O_3$	32.6
Reduced $0.7AuFe_2O_3$	9.9
Fe_2O_3	100.7

[a]Sample properties in table 2.

3.2. CO oxidation on Au/Fe_2O_3

Haruta *et al.* first showed the extremely high CO oxidation activity of Au on Fe_2O_3, with appreciable conversions measured at −70 °C in a gas composed of 1%CO in air [1,18]. The hypothesis was that very finely dispersed gold created a large number of interfacial gold ions, which along with the metallic gold sites contributed to activity. In a more recent examination of this type catalyst, Hutchings *et al.* [29] have claimed that gold cations are key for an active catalyst. However, their samples always contained a mixture of both gold nanoparticles and gold ions. Here, we take another look at Au/Fe_2O_3 catalysts, making sure we have a sample that contains exclusively ionic gold, as is possible by leaching. As parent, the reference catalyst (2 at.% Au/Fe_2O_3) supplied by the World Gold Council was used. The derived leached material contained 0.7 at.%Au (table 2).

Figure 4 shows the CO oxidation light off curves for the parent and leached Au/Fe_2O_3. In each experiment, 90 mg of material was used and the space velocity was 100,000/h. The support Fe_2O_3 itself becomes active for this reaction only above 250 °C. The reaction on the parent catalyst with 2%Au lights off far below room temperature, while on the leached catalyst with 0.7%Au, it does not light off until 150 °C is reached. However, after this sample was reduced by hydrogen from room temperature to 400 °C, it became very active, similar to the parent catalyst even though some deactivation was also observed.

The parent catalyst comprises both zerovalent gold and oxidized gold species as characterized by UV–Vis in figure 5. The spectrum of the series Au/Fe_2O_3 exhibited a broad band with maximum at ca. 245 nm, which can be assigned to electronic transition of d–d type in the Fe^{3+} ion and is ascribed to the $E_g \rightarrow T_{2g}$ transition [53,54]. For those samples that did not undergo further reactions, an absorption band at about 385 nm can be observed, which corresponds to oxidized states of gold in the form of Au^+ and $Au_n^{\delta+}$ [55]. The metallic gold peak, known to be located between 520–570 nm for gold particles on metal oxides [28,56] is found only on the

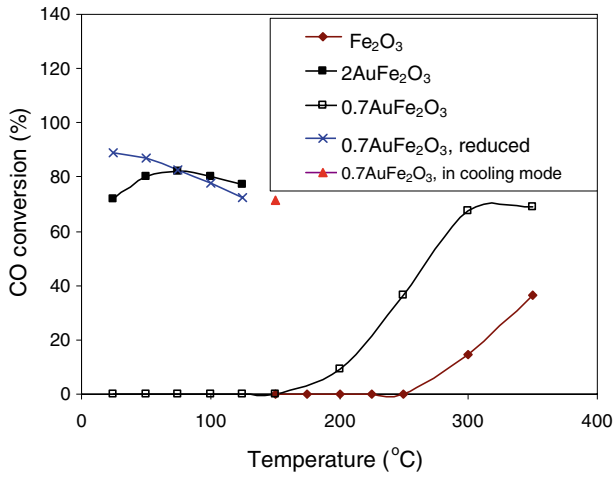

Figure 4 CO conversion in the CO oxidation over gold–iron oxide catalysts. Gas mixture: 2%CO-1%O_2-balance He; Space velocity: 100,000/h.

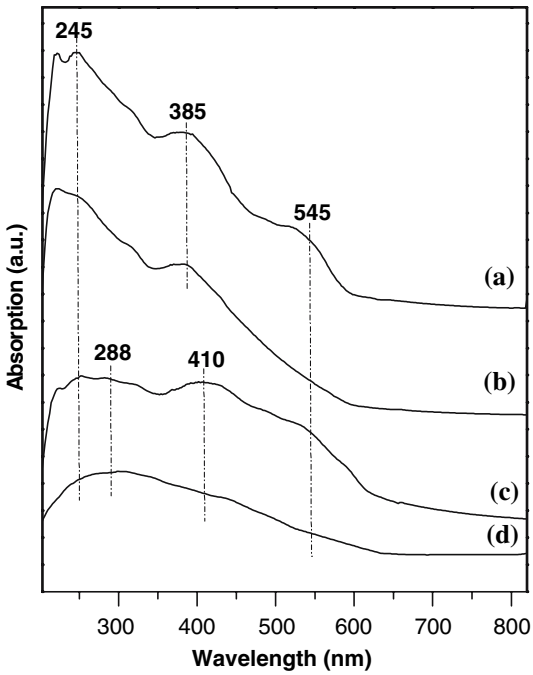

Figure 5 UV–Vis spectra of Au/Fe_2O_3 samples in ethanol: (a) $2Au/Fe_2O_3$; (b) $0.7\ Au/Fe_2O_3$; (c) $0.7\ Au/Fe_2O_3$, reduced in H_2 up to 400 °C; (d) Fe_2O_3.

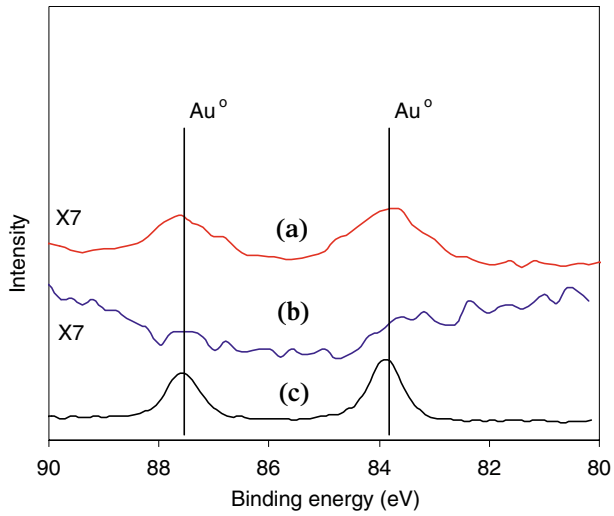

Figure 6 XP spectra of Au_{4f} in as-prepared and reduced gold–iron oxide catalysts. X7 represents signal magnification (a) $0.7\ Au/Fe_2O_3$, reduced in H_2 up to 400 °C; (b) $0.7\ Au/Fe_2O_3$; (c) $2Au/Fe_2O_3$.

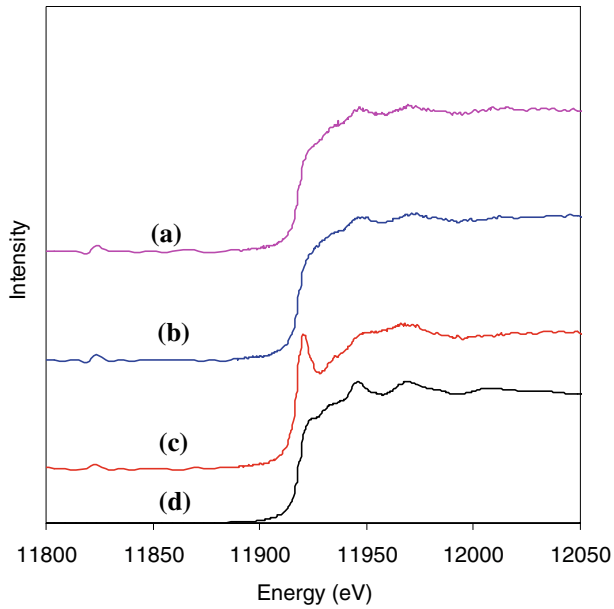

Figure 7 XANES of $0.7AuFe_2O_3$: (a) $0.7Au/Fe_2O_3$, after CO oxidation up to 350 °C (see figure 4); (b) $0.7Au/Fe_2O_3$, reduced in hydrogen up to 400 °C; (c) $0.7Au/Fe_2O_3$; (d) reference material Au foil.

parent catalyst. This disappeared after the NaCN leaching. For the leached sample exposed to hydrogen up to 400 °C, the whole spectrum changes greatly from that of the fresh material. Besides the absorption typically observed for Fe^{3+}, one broad band centered at about 410 nm was found in figure 5 (c). This band may be attributed to absorption of bulk gold from intrinsic photo-effect, while at the same time, we cannot ignore the possibility of Fe^{3+} ions in aggregated form (e.g. iron hydroxide clusters in the experimental conditions) [54]. It has been reported that the broad peak at around 400 nm is due to iron hydroxide clusters [54]. The appearance of the band at ~545 nm in spectrum c of figure 5 clearly indicates that metallic gold species form upon hydrogen reduction.

XP spectra of Au_{4f} of gold–iron oxide samples are shown in figure 6. For the leached $0.7AuFe_2O_3$ no detectable gold signal was obtained, probably due to the fact that gold is embedded. However, the presence of oxidized gold in the iron oxide sample was confirmed by XANES. In figure 7, the XANES spectrum of fresh leached $0.7AuFe_2O_3$ shows the characteristic features of oxidized gold [30]. As shown in figure 4, this sample has no activity for the CO oxidation reaction up to 150 °C, apparently because of the loss of active sites due to the removal of gold from the surface by the sodium cyanide treatment. Sze *et al.* proposed that Au can substitute into the Fe_2O_3 unit cell as ions in +3 oxidation state as evidenced by XPS and Mossbauer spectroscopy [57]. Haruta *et al.* [58] explained that an intermetallic bond is formed between Fe and Au, as supported by the slight solubility of Fe in Au and the Au–Fe distance. Our results show that the gold embedded in the iron oxide lattice is stable to heating in air to 400 °C, as confirmed by XPS (line b in figure 6). The $0.7AuFe_2O_3$ sample shows no gold species on the surface and subsurface, most probably due to the shielding from the big size of iron oxide particles (25.6 nm). Reduction in hydrogen at 400 °C, however, succeeds in bringing the gold clusters to the surface, as found by XPS, line a in figure 6. The reduction of gold is also confirmed by the XANES analysis of the reduced sample in line b of figure 7.

There is a clear hysteresis in the CO light-off tests on $0.7AuFe_2O_3$, figure 4. After testing at 350 °C and continued testing in cooling mode, the CO conversion was 71.5% at 150 °C, compared to zero conversion measured in the ascending temperature mode. Thus, the reaction mixture can activate (reduce) the gold. To demonstrate the reduction effect more clearly, the $0.7AuFe_2O_3$ sample was reduced in hydrogen from room temperature to 400 °C, upon which it became very active. A dramatic enhancement of activity is observed in figure 4 for the pre-reduced material, indicative of extensive surface structure changes. As shown by UV–Vis (figure 5, line c), XPS (figure 6, line a) and XANES (figure 7, line b), reduction of gold took place and the embedded gold was brought out to the surface of the sample. On the contrary, heating in air at 400 °C left the gold ions in the sample. This is interesting, as it demonstrates the high stability of the Au–O–Fe state. Indeed, recent work by Guczi *et al.* has shown that depositing a thin film of FeOx that completely covers a Au film results in an active catalyst for CO oxidation at 803 K [59]. They attributed the enhanced catalytic activity of the $FeOx/Au/SiO_2/Si$ (100) to active sites located on the iron oxide overlayer promoted by the gold underneath. It was proposed that during the reaction Au atoms diffuse into the iron oxide layer owing to elevated temperature but do not seem to reach the surface because TOF secondary ion mass spectrometry did not detect any Au^+ emission from the surface of the used sample. However XPS analysis of the $FeOx/Au$ layer/$SiO_2/Si(1\ 0\ 0)$ sample used for 1 h-on-stream in CO oxidation reaction found Au 4f signal while there was no Au signal before reaction, which is consistent with our XPS data. The surface of active catalysts is dominated by Au^o. Moreover, hydrogen reduction or CO/O_2 gas can bring the embedded gold out to the surface of iron oxide with concomitant large activity enhancement.

To quantify this enhancement, we conducted kinetic measurements of the CO oxidation reaction on the various samples tested in figure 4. Arrhenius-type plots for the reaction rates are shown in figure 8. First, the parent $2AuFe_2O_3$ catalyst is much more active than the leached $0.7AuFe_2O_3$, which has most of its gold embedded as discussed above. However, the latter is still more active than the unmodified, gold-free Fe_2O_3 or its reduced derivative, Fe_3O_4. Figure 8 and table 4 show that the apparent activation energy of the reaction increases from 13.4 kJ/mol for the parent sample to 32.6 kJ/mol for the leached sample. The latter agrees with what has been reported by Haruta *et al.* for a low-content $Au–Fe_2O_3$ sample prepared by coprecipitation, table 1, Ref. 18. By removing the metallic gold, the reaction pathway has changed. Reduction of the leached sample improved its activity dramatically. Thus, at 30 °C, the reaction rate was 14.8 $\mu molCO/g_{cat}/s$ for the reduced $0.7AuFe_2O_3$ and 8.9 $\mu molCO/g_{cat}/s$ for the

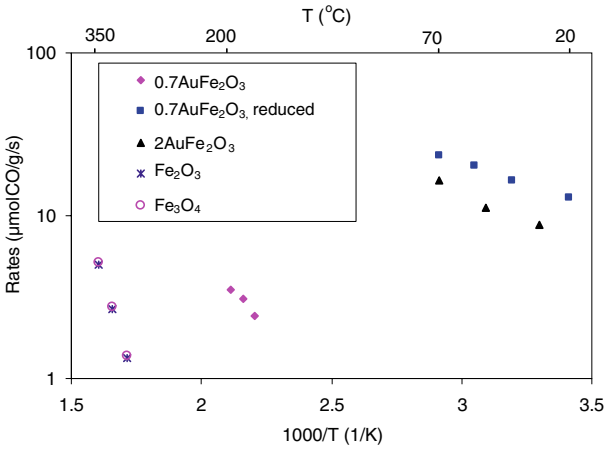

Figure 8 Steady-state CO oxidation reaction rates over gold–iron oxide catalysts measured in a gas composed of 2%CO-1%O_2-balance He. Flow rate: 150mL/min.

parent $2AuFe_2O_3$. Taking into account the different amount of gold in these two samples, we can surmise that the dispersion of gold in the reduced leached sample is much higher (probably close to 100%) than that of the parent. This would give the same turnover frequency with proper scaling of the active sites. Another way to state this is that the number of active sites for CO oxidation on the gold clusters of the pre-reduced sample is higher than on the gold particles of the parent. The activity of the reduced $0.7AuFe_2O_3$ catalyst is comparable to the most active CO oxidation catalysts Au/TiO_2 [4] and $Au/Fe(OH)_3$ [50] reported in the literature (table 1) which were tested in a gas mixture composed of 1%CO and 20%O_2.

In exploring potential reaction pathways, it is possible that CO weakly bound to gold nanoparticles will react readily with oxygen adsorbed on cus sites of gold [36], the oxygen coming from the gas phase or from the support, to form CO_2 [60]. On the other hand, oxidation is hindered when CO is more strongly adsorbed on oxidized $Au_n^{\delta+}$, as shown by FTIR for the $Au–CeO_2$ system [51]. A different pathway, often proposed but not proven in the literature, involves CO adsorbed on Au(0) sites and interacting with –OH groups at the interface with the oxide support on non-heat treated samples. This carboxylate binds with a superoxide and forms CO_2 [61]. As more evidence keeps accumulating on the high CO oxidation activity of gold nanoparticles on any oxide support, including a recent study on SiO_2 [62] and even on non-oxide supports [16], the mechanistic options appear to zero in to highly defective gold clusters independent of the support.

3.3. *The WGS reaction on Au/CeO_2 and Au/Fe_2O_3*

It is clear from the results presented above that the low temperature CO oxidation over $Au–CeO_2$ and

$Au–Fe_2O_3$ is a much more facile reaction on gold nanoparticles than on oxidized gold clusters. On the other hand, we have reported that on Au/CeOx only the gold species strongly interacting with ceria, [Au_n–O–Ce], are needed to activate the WGS reaction; while gold nanoparticles are spectator species for this reaction [22,23]. Here we consider the case of the WGS reaction on the gold–ceria and gold–iron oxide supports examined above to explore the similarities or differences between these two systems.

Previous work [23,63] from our lab has shown that the oxidation state of gold depends on the reaction gas composition. First, reversible gold structures were observed in mildly reducing WGS conditions, while in more reducing gas mixtures, more gold reduction took place and at high enough temperatures (> 250 °C), gold sintering and irreversible loss of activity took place. For the WGS reaction in this study, we conducted steady-state light off tests in a product-free gas mixture (2%CO-10.7%H_2O-He), figure 9, and steady-state rate measurements in a simulated reformate gas mixture (11%CO-26%H_2O-26%H_2-7%CO_2-He), figure 10. The leached 0.5AuCL and 0.7$AuFe_2O_3$ catalysts have similar activity as the parent catalysts for the WGS reaction. It is noted that the WGS simulated-reformate gas has a similar effect on gold mobility as the CO oxidation gas mixture we discussed above, which can bring the embedded gold from the bulk to the surface. XPS analysis shows that the surface concentration of Au increased from zero to 1.75 at.% for the used 0.7$AuFe_2O_3$ (after the WGS rate measurement in figure 10). The apparent activation energy of the WGS reaction over both catalysts is the same, 49 ± 7 kJ/mol. Unlike the CO oxidation reaction, leaching of the gold from the parent catalysts does not affect the reaction rate. Therefore, additional metallic gold nanoparticles present in the parent catalysts do not participate in this reaction. Furthermore, when the leached 0.5AuCL was reduced in 20%H_2 from room temperature to 400 °C (*in situ*), the CO conversions for this material were lower than the fresh material, indicating that the oxidized Au is more active for the WGS reaction. The active sites are thus the oxidized [Au–O–Ce] and [Au–O–Fe] species on the surface and subsurface layers of these catalysts.

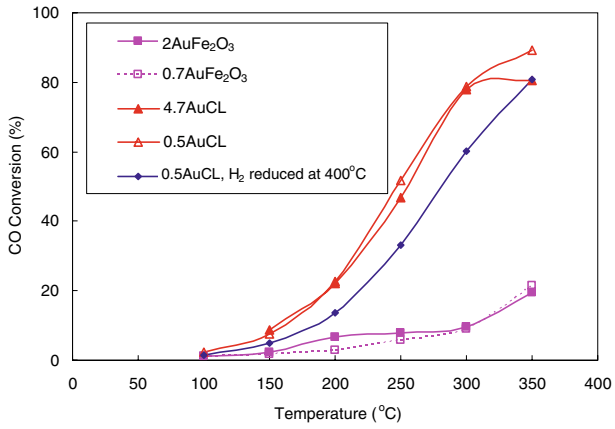

Figure 9 WGS reaction light-off curves over gold–ceria and gold–iron oxide catalysts; measured at steady-state. Gas mixture: 2%CO-10.7%H_2O-He; contact time: 0.09 g s/cc.

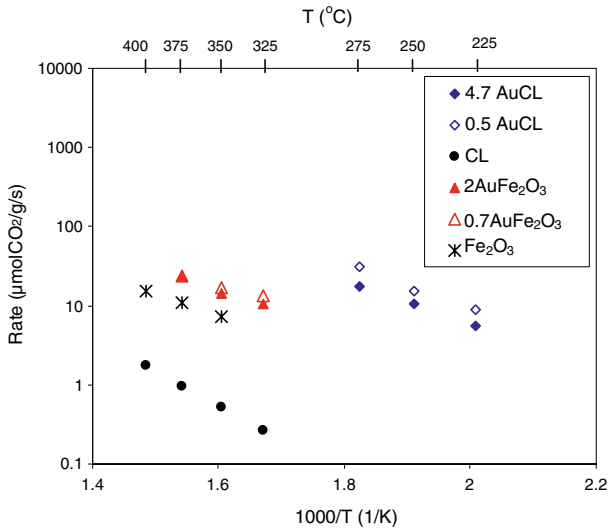

Figure 10 WGS activities of parent and leached gold–ceria and gold–iron oxide catalysts. Gas mixture: 11%CO-26%H_2O-26%H_2-7%CO_2-He. Flow rate: 207 mL/min.

Mechanistically, we may understand the difference from the case of dry CO oxidation as one where the activation of the oxygen species involved in this reaction (–OH groups) is harder to accomplish. Hence, only the strongly bound CO on oxidized gold clusters is a participant in the reaction pathway. In previous work, CO-TPR was used to demonstrate that H_2 was formed at the same temperature (~100 °C) on both the parent and leached AuCeOx catalysts [22]. Hydrogen formation coincided with the onset of consumption of the first of the two surface oxygen species of ceria, while the oxygen adsorbed on Au^o produced CO_2 only. Thus, spillover of oxygen species from the support onto the gold particle surfaces does not appear to be operative in these systems. Otherwise the activity of the parent catalysts would be much higher than that of the leached ones, but this is not the case, as shown in figure 10 by comparison of the reactivity of 4.7AuCL and 0.5AuCL samples. We propose that the strongly adsorbed CO on the $Au_n^{\delta+}$ clusters begins to react with a neighboring –OH of ceria at ~100 °C, as shown by the onset of H_2 production in CO-TPR [22] and by the reaction light off profiles in figure 9. The weakly bound CO on metallic gold is not a contributor to this reaction. In addition, and very significantly, the Au/Fe_2O_3 and Au/CeO_2 have very similar activity, figure 10, if we scale the rates by the surface area of each support, table 2.

4. Conclusions

The dry CO oxidation reaction is much more facile on Au^o than on oxidized gold clusters, as found here for both $Au–CeO_2$ and $Au–Fe_2O_3$ catalysts. XANES, XPS, TPR and UV–Vis analyses show that reduction of the leached samples containing oxidized gold only is needed to activate the catalyst. This can be accomplished by pre-reduction in hydrogen or by long exposure to the CO/O_2 reaction gas mixture at temperatures above 125 °C for $AuCeO_2$ or 350 °C for $AuFe_2O_3$. Well dispersed metallic gold nanoparticles provide the active sites for the low temperature CO oxidation reaction on both CeO_2 and Fe_2O_3. On the other hand, the WGS reaction lights off above 100 °C, similarly for the parent samples containing both gold nanoparticles and oxidized gold species or their derivatives prepared by leaching out the weakly bound gold, and containing only the strongly bound oxidized gold species. The WGS reaction activation energy is the same over $Au–CeO_2$ and $Au–Fe_2O_3$, 49 ± 7 kJ/mol. This points to activation of –OH from the oxide support and the strongly bound CO on $Au^{\delta+}$ as a plausible mechanism for this reaction.

Acknowledgment

This work was supported by the National Science Foundation, NIRT Grant # 0304515; and by the Department of Energy, Basic Energy Sciences, Hydrogen Fuel Initiative Grant # DE-FG02-05ER15730. The use of the synchrotron radiation for the XAS experiments at the NSLS (Brookhaven National Lab) is acknowledged. The NSLS is supported by the Divisions of Chemical and Materials Science of the U.S. Department of Energy.

References

[1] M. Haruta, N. Yamada, T. Kobayashi and S. Iijima, J. Catal. 115 (1989) 301.
[2] A.K. Sinha, S. Seelan, M. Okumura, T. Akita, S. Tsubota and M. Haruta, J. Phys. Chem. B 109 (2005) 3956.
[3] G.C. Bond and D.T. Thompson, Appl. Catal. A 302 (2006) 1.
[4] G.R. Bamwenda, S. Tsubota, T. Nakamura and M. Haruta, Catal. Lett. 44 (1997) 83.
[5] M. Valden, X. Lai and D.W. Goodman, Science 281 (1998) 1647.
[6] V. Schwartz, D.R. Mullins, W. Yan, B. Chen, S. Dai and S.H. Overbury, J. Phys. Chem. B 108 (2004) 15782.
[7] S.H. Overbury, V. Schwartz, D.R. Mullins, W. Yan and S. Dai, J. Catal 241 (2006) 56.
[8] S.D. Gardner, G.B. Hoflund, D.R. Schryer, J. Schryer, B.T. Upchurch and E.J. Kielin, Langmuir 7 (1991) 2135.
[9] W. Liu and M. Flytzani-Stephanopoulos, J. Catal. 153 (1995) 304.
[10] W. Liu and M. Flytzani-Stephanopoulos, J. Catal. 153 (1995) 317.
[11] S. Carrettin, P. Concepción, A. Corma, J.M.L. Nieto and V.F. Puntes, Angew. Chem. Int. Ed. 43 (2004) 2538.
[12] M. Okumura, S. Nakamura, S. Tsubota, T. Nakamura, M. Azuma and M. Haruta, Catal. Lett. 51 (1998) 53.
[13] C.K. Costello, J.H. Yang, H.Y. Law, Y. Wang, J.-N. Lin, L.D. Marks, M.C. Kung and H.H. Kung, Appl. Catal. A 243 (2003) 15.
[14] J.T. Calla and R.J. Davis, Catal. Lett. 99(1–2) (2005) 21.
[15] N. Weiher, E. Bus, L. Delannoy, C. Louis, D.E. Ramaker, J.T. Miller and J.A. van Bokhoven, J. Catal. 240 (2006) 100.
[16] W. Yan, S. Brown, Z. Pan, S.M. Mahurin, S.H. Overbury and S. Dai, Angew. Chem. Int. Ed. 45 (2006) 3614.
[17] a: M.M. Schubert, A. Venugopal, M.J. Kahich, V. Plzak, R.J. Behm, J. Catal. 222 (2004) 32; b: M.M. Schubert, V. Plzak, J. Garche, R.J. Behm, Catal. Lett. 76 (2001) 143.
[18] M. Haruta, S. Tsubota, T. Kobayashi, H. Kageyama, M.J. Genet and B. Delmon, J. Catal. 144 (1993) 175.
[19] W. Deng, J. De Jesus, H. Saltsburg and M. Flytzani-Stephanopoulos, Appl. Catal. A 291 (2005) 126.
[20] Q. Fu, A. Weber and M. Flytzani-Stephanopoulos, Catal. Lett. 77(1–3) (2001) 87.
[21] H.C. Yao and Y.F.Y. Yao, J. Catal. 86 (1984) 254.
[22] Q. Fu, H. Saltsburg and M. Flytzani-Stephanopoulos, Science 301 (2003) 935.
[23] Q. Fu, W. Deng, H. Saltsburg and M. Flytzani-Stephanopoulos, Appl. Catal. B 56 (2005) 57.
[24] E.S. Putna, R.J. Gorte, J.M. Vohs and G.W. Graham, J. Catal. 178 (1998) 598.
[25] S. Carrettin, A. Corma, M. Iglesias and F. Sánchez, Appl. Catal. A. 291(1–2) (2005) 247.
[26] P. Concepción, S. Carrettin and A. Corma, Appl. Catal. A 307 (2006) 42.
[27] J. Guzman, S. Carrettin, J.C. Fierro-Gonzalez, Y. Hao, B.C. Gates and A. Corma, Angew. Chem. Int. Ed. 44 (2005) 4778.
[28] Guzman J., Corma A. (2005) Chem Comm. 743.
[29] G.J. Hutchings, M.S. Hall, A.F. Carley, P. Landon, B.E. Solsona, C.J. Kiely, A. Herzing, M. Makkee, J.A. Moulijn, A. Overweg, J.C. Fierro-Gonzalez, J. Guzman and B.C. Gates, J.Catal. 242 (2006) 71.
[30] J. Guzman and B.C. Gates, J. Phys. Chem. B 106 (2002) 7659.
[31] J.C. Fierro-Gonzalez and B.C. Gates, Langmuir 21 (2005) 5693.
[32] M.S. Chen and D.W. Goodman, Science 306 (2004) 252.
[33] M.S. Chen and D.W. Goodman, Catal. Today 111 (2006) 22.
[34] C.T. Campbell, Science 306 (2004) 234.
[35] S. Lai, Y. Qiu and S. Wang, J. Catal. 237 (2006) 303.
[36] I.N. Remediakis, N. Lopez and J.K. Nørskov, Appl. Catal. A 291(1–2) (2005) 13.
[37] X. Wang, J.A. Rodriguez, J.C. Hanson, M. Pérez and J. Evans, J. Chem. Phys. 123 (2005) 221101.
[38] D. Tibiletti, A. Amieiro-Fonseca, R. Burch, Y. Chen, J.M. Fisher, A. Goguet, C. Hardacre, P. Hu and D. Thompsett, J. Phys. Chem. B 109(47) (2005) 22553.
[39] Z.-P. Liu, S.J. Jenkins and D.A. King, Phys. Rev. Lett 94 (2005) 196102.
[40] M.A. Bollinger and M.A. Vannice, Appl. Catal. B 8 (1996) 417.
[41] J.D. Grunwaldt and A. Baiker, J. Phys. Chem. B 1073 (1999) 1002.
[42] J.H. Yang, J.D. Henao, M.C. Raphulu, Y. Wang, T. Caputo, A.J. Groszek, M.C. Kung, M.S. Scurrell, J.T. Miller and H.H. Kung, J. Phys. Chem. B 109(20) (2005) 10319.
[43] D. Wang, Z. Hao, D. Cheng, X. Shi and C. Hu, J. Mol. Catal. A 200 (2003) 229.
[44] U.R. Pillai and S. Deevi, Appl. Catal. A 299 (2006) 266.
[45] Tz. Venkov, Hr. Klimev, M.A. Centeno, J.A. Odriozola and K. Hadjiivanov, Catal. Comm. 7(5) (2006) 308.
[46] Y. Li, Q. Fu and M. Flytzani-Stephanopoulos, Appl. Catal. B 27 (2000) 179.
[47] Y. Yuan, P. Kozlova, K. Asakura, H. Wan, K. Tsai and Y. Iwasawa, J. Catal. 170 (1997) 191.
[48] A.M. Venezia, G. Pantaleo, A. Longo, G.D. Carlo, M.P. Casaletto, F.L. Liotta and G. Deganello, J. Phys. Chem. B 109 (2005) 2821.
[49] J. De Jesus, M.S thesis, Chemical & Biological Engineering, Tufts University, 2004.
[50] Q. Fu, S. Kudriavtseva, H. Saltsburg and M. Flytzani-Stephanopoulos, Chem. Eng. J. 93 (2003) 41.

[51] M. Manzoli, F. Boccuzzi, A. Chiorino, F. Vindigni, W. Deng and M. Flytzani-Stephanopoulos, J. Catal. 245 (2007) 306.
[52] Y. Wu, E. Garfunkel and T.E. Madey, J. Vac. Sci. Technol. A 14 (1996) 1662.
[53] M.M. Abou-Sekkina, M.M. El-Kersh and O.A. Shalma, J. Radioanal. Nucl. Chem. 241 (1999) 15.
[54] P. Marturano, L. Drozdovâ, G.D. Pirngruber, A. Kogelberger and R. Prins, Phys. Chem. Chem. Phys. 2 (2001) 5585.
[55] A.N. Pestryakov, V.V. Lunin, A.N. Kharlanov, D.I. Kochubey, N. Bogdanchikova and A.Y. Stakheev, J. Mol. Struct. 642 (2002) 129.
[56] A.N. Pestryakov, V.V. Lunin, A.N. Kharlanov, N.E. Bogdanchikova and I.V. Tuzovskaya, Eur. Phys. J. D 24 (2003) 307.
[57] C. Sze, E. Gulari and B.G. Demczyk, Mater. Lett. 36 (1998) 11.
[58] M. Haruta, T. Kobayashi, S. Iijima, F. Delannay, in: *Proceedings 9th Int. Congr. Catal., Calgary, 2*, eds. M.J. Phillips and M Ternan, (The Chemical Institute of Canada, Ottawa, 1988) p. 1206.
[59] L. Guczi, K. Frey, A. Beck, G. Petõ, C.S. Daroóczi, N. Kruse and S. Chenakin, Appl. Catal. A 291 (2005) 116.
[60] H. Liu, A.I. Kozlov, A.P. Kozlova, T. Shido and Y. Iwasawa, Phys. Chem. Chem. Phys. 1 (1999) 2851.
[61] G.C. Bond and D.T. Thompson, Catal. Rev. Sci. Eng. 41 (1999) 319.
[62] H. Zhu, C. Liang, W. Yan, S.H. Overbury and S. Dai, J. Phys. Chem. B 110 (2006) 10842.
[63] W. Deng, Ph.D thesis, Tufts University, in progress.